 doi:10.20944/preprints202208.0075.v1

Article

Waste Plastic Direct Extrusion Hangprinter

Aliaksei Petsiuk [1], Bharath Lavu [2], Rachel Dick [2] and Joshua M. Pearce [1,2,3,*]

[1] Department of Electrical & Computer Engineering, Western University, ON, Canada; apetsiuk@uwo.ca
[2] Department of Materials Science & Engineering, Michigan Technological University, MI, US; blavu@mtu.edu; redick@mtu.edu
[3] Ivey Business School, Western University, London, ON, Canada; joshua.pearce@uwo.ca

* Correspondence: joshua.pearce@uwo.ca

Abstract: As the additive manufacturing industry grows, it is compounding the global plastic waste problem. Distributed recycling and additive manufacturing (DRAM) offers an economic solution to this challenge, but it has been relegated to either small-volume 3D printers (limiting waste recycling throughput) or expensive industrial machines (limiting accessibility and lateral scaling). To overcome these challenges, this paper provides proof-of-concept for a novel open-source hybrid 3D printer that combines a low-cost hanging printer design with a compression screw-based end-effector that allows direct extrusion of recycled plastic waste in large expandable printing volumes. Mechanical testing of the resultant prints from 100% waste plastic, however, showed that combining challenges of non-uniform feedstocks and a heavy printhead for a hangprinter reduced the strength of the parts compared to fused filament fabrication. The preliminary results are technologically promising, however, and provide opportunities to improve on the open source design to help process the volumes of waste plastic needed for DRAM to address the negative environmental impacts of global plastic use.

Keywords: 3D printing; additive manufacturing; big area additive manufacturing; BAAM; hanging printer; hangprinter; plastic waste; recycling; sustainable manufacturing; wire robot

1. Introduction

The problem of plastic waste recycling [1] is compounded by the popularity of 3D printing, which stimulates experimental design and innovations, while increasing the number of defective parts and waste products [2]. Although the first self-replicating open source 3D printer [3] created an explosion of innovation and reduced costs for additive manufacturing (AM), a significant and increasing amount of plastic waste produced by 3D printers is dumped in landfills around the world [4]. According to the economic forecasts, the global 3D printing market is going to reach $7.7 billion by 2024 [5].

To reach a circular economy for plastic in the additive manufacturing (AM) industry [6,7], a profitable and rapidly growing approach to increasing recycling rates is distributed recycling for additive manufacturing (DRAM) [8-10]. Producing consumers (or prosumers) have an economic incentive based on savings for recycling with DRAM, as opposed to the traditional recycling model where they do not [8]. Prosumers can use their waste as raw material for 3D printing feedstocks, which is a relatively high value for plastic (e.g. $20/kg). In the most environmentally-friendly version of DRAM [11,12], prosumers manufacture their own products from the 3D printing feedstocks [13] making a high return on investment [14]. Thus, as DRAM is applicable globally [15], it has the potential to radically impact global value chains [16].

The majority of past research on DRAM has focused on using some form of recyclebot (waste plastic extruder) [17,18] to provide raw materials for fused filament fabrication (FFF) used for low-cost RepRap-class 3D printers. Recently, however, there has been rapid development in direct extrusion waste 3D printing via fused granular fabrication

Preprints (www.preprints.org) | NOT PEER-REVIEWED | Posted: 3 August 2022 doi:10.20944/preprints202208.0075.v1

(FGF)/fused particle fabrication (FPF) [19-23]. Although FPF/FGF is possible on the desktop [24], it is particularly well-suited for large prints [25].

The rigid mechanical design of most 3D printers limits the size of the print, and the need to increase the volume of printed parts leads to expansion of the entire machine, which significantly increases capital costs. Today's high-volume 3D printers are expensive, have rigid frames, and require a lot of assembly (Table 1) [26-35], with the one exception of the open source hangprinter [35].

Table 1. Comparison of cost and print volume of existing large 3D printers.

Name	Price, USD	Printing volume
Gigabot XLT (re3d) [26]	16,995	590x760x900 mm
Exabot (re3d) [27]	85,000	762x762x1,829 mm
Terabot (re3d) [28]	34,400	915x915x1000 mm
THE BOX Large (BLB Industries) [29]	298,000	2000×2000×1500 mm
T3500 (Tractus3D) [30]	59,000	⌀1000x2100 mm
400 Series Workbench Extreme (3D Platform) [31]	50,000	1000×1500×700 mm
BIG-Meter (Modix) [32]	11,500	1010×1010×1010 mm
BigRep ONE v4 (BigRep) [33]	30,000	1005×1005×1005 mm
F1000 (CreatBot) [34]	30,000	1000×1000×1000 mm
Hybrid Hangprinter (open source) [35]	<1,200	Expandable over a wide dimensional range

The hangprinter is an open source cable driven 3D printer. The first version of the hangprinter was released by Ludvigsen and Kracht in 2006 based on existing market limitations [35]. The hangprinter design belongs to the category of wire, or cable, robots, which are well understood [36-41]. Similar large-scale experimental printers include Arcus-3D-C1 [42], Sensorica's SpiderRig [43], and Trikarus [44].

Using the hanging cable-based 3D printer approach, allows changing the printing scale upon request with virtually no additional components. This study focuses on the concept of using recycled material for AM and big area additive manufacturing (BAAM) by implementing a low-cost open-source hybrid 3D printer design based on hangprinter and FPF/FGF print head. This approach has the potential to create a considerable advantage for DRAM by reducing design constraints and capital costs, while increasing recycling volumes. The developed hybrid printer relies entirely on cabled connections without a rigid frame and can be built into existing structures such as interior and exterior parts of buildings or suspended from any type of anchor points. The system is designed, prototyped and tested for both positional accuracy and the mechanical strength of parts fabricated from recycled plastic with the system. The results are presented and discussed in the context of DRAM.

2. Method

2.1. Hybrid printer design

Since the release of the first version of the hangprinter, the mechanical hardware and software have undergone several improvements35. Version 3 of the hangprinter45 uses Nema 17 motors and a standard 3D printing extrusion kit controlled by a modified Marlin firmware [46] on an Arduino Mega board. The developed hybrid printer (Figure 1) uses more powerful Nema 23 stepper motors to carry the heavier end effector with the direct print FPF/FGF extruder.

Preprints (www.preprints.org) | NOT PEER-REVIEWED | Posted: 3 August 2022 doi:10.20944/preprints202208.0075.v1

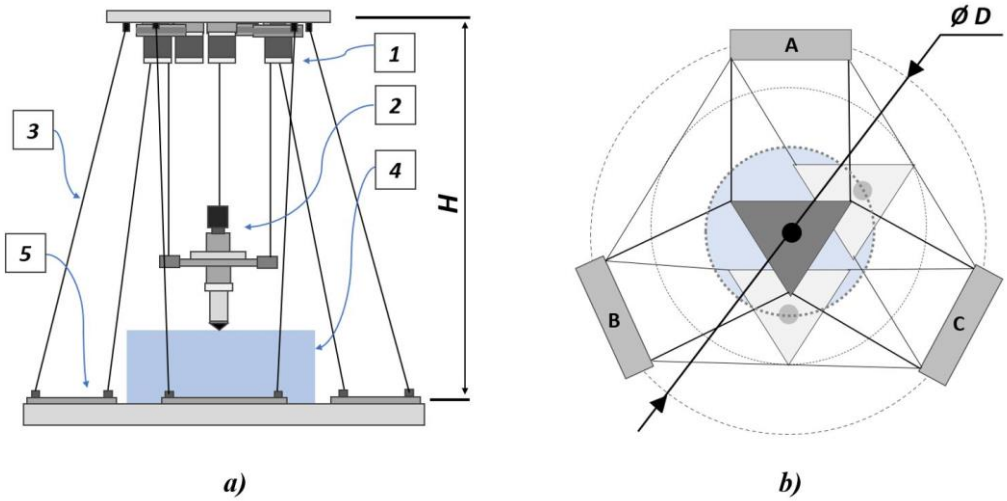

Figure 1. Scheme of the hybrid printer. a) side view, b) top view. 1 – ceiling unit, 2 – effector (FPF/FGF extruder), 3 – wires, 4 – cylindrical working volume, 5 – printing bed, A, B, and C – anchors; H = 190 cm (height of the printer), ØD = 140 cm (diameter of the lower part of the printer).

Gears, spools, anchors, linear rollers, carriage holders, and motor mounting brackets included with the printer are 3D printed. The ceiling unit and anchors are attached to plywood, while the room floor can be used as the printing surface. Motor gears and bracket mounts, carriage beam holders, level sliders, and end effector case have been customized [47] to suit the existing load.

The electrical connection diagram is shown in Figure 2. This hybrid printer setup uses five (A, B, C, D, and E) Nema 23 stepper motors with TB6600 drivers and a 3D printing kit based on the RAMPS 1.4 controller [48]. The heating system of the screw extruder consists of four parallel 12V/60W heating elements combined into two heating zones. The entire electrical system is powered by a 12V power supply.

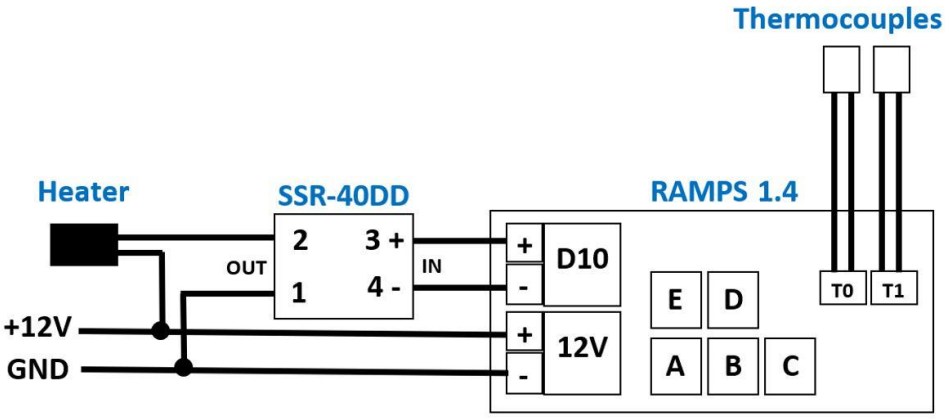

Figure 2. Hybrid printer wiring diagram.

The assembled and mounted hybrid hangprinter is shown in Figure 3. A triangular frame, made up of three 40 cm aluminum channels, carries the waste plastic extruder. The braided string with a breaking strength of 22.7 kgs is used as a wire for the assembly.

Preprints (www.preprints.org) | NOT PEER-REVIEWED | Posted: 3 August 2022 doi:10.20944/preprints202208.0075.v1

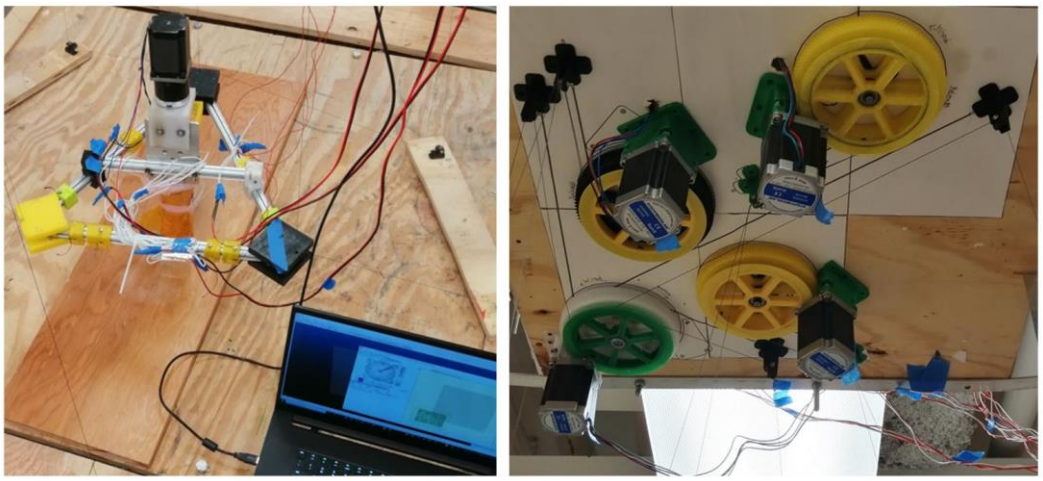

a) b)

Figure 3. Hybrid printer assembly. a) end effector (FPF/FGF extruder) and the printing bed with A, B, and C anchors, b) ceiling unit with gears, motors, and line rollers.

2.2. Firmware and calibration

The hybrid printer is controlled by the modified Marlin firmware where several G- and M-code commands were adapted to use ABCD coordinates instead of the traditional XYZ (Figure 4).

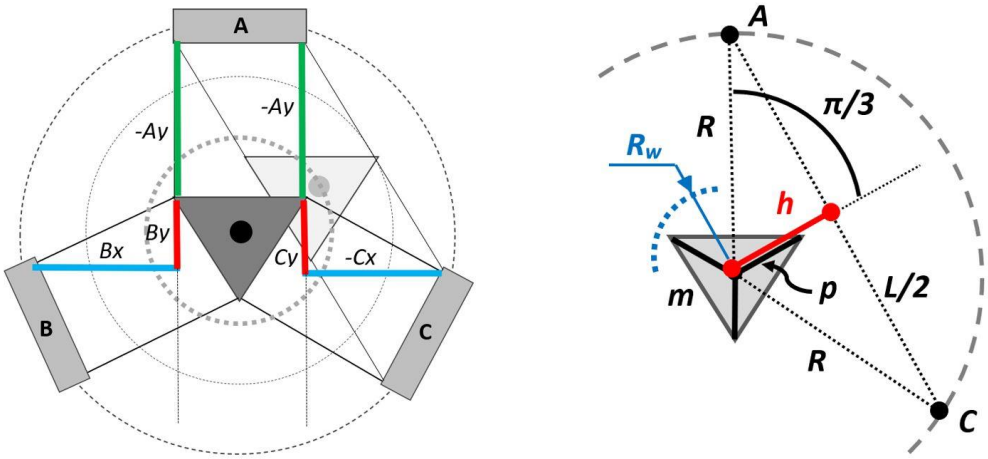

a) b)

Figure 4. Calibration parameters and geometric constraints of the hybrid printer. a) calibration parameters, b) End effector movement constraints: R_w – radius of the printing (working) zone, R – distance between the anchor and the geometric center of the print surface, h – distance to the AC chord, p – distance to the mass center of the equilateral triangle (nozzle support structure), L – length of the AC chord, m – nozzle support structure side length, and $\pi/3$ – half of the central angle.

Parallel wires prevent the end effector from rotating around its own axis while moving along a given G-code path. The firmware cuts the G-code trajectories into straight line segments, each of which is calculated according to the following equation (1) [35]:

$$\begin{cases} l_A = \sqrt{(P_X - A_X)^2 + (P_Y - A_Y)^2} \\ l_B = \sqrt{(P_X - B_X)^2 + (P_Y - B_Y)^2} \\ l_C = \sqrt{(P_X - C_X)^2 + (P_Y - C_Y)^2} \end{cases} \quad (1)$$

Preprints (www.preprints.org) | NOT PEER-REVIEWED | Posted: 3 August 2022 doi:10.20944/preprints202208.0075.v1

Where l_A, l_B, and l_C —are the line segments for the corresponding anchors, (P_X, P_Y)—coordinates of the end effector, and $(A_X, A_Y, B_X, B_Y, C_X, C_Y)$—coordinates of the anchors A, B, and C, respectively.

In the assembled system, the following parameters were added to the firmware, obtained by calibrating the printer geometry (Figure 4a):

- Ay = -475 mm
- Bx = 395 mm
- By = 163 mm
- Cx = -460 mm
- Cy = 300 mm
- Dz = 1900 mm (distance from the printing surface to the line rollers on the ceiling unit)

The print area radius R_w (Figure 4b) can be calculated using the following equation (2):

$$h = \sqrt{R^2 - \frac{L^2}{4} = R^2 - 4R^2 \cdot sin^2\left(\frac{\pi}{3}\right)} = R \cdot cos\left(\frac{\pi}{3}\right)$$
$$R_w = h - p = R \cdot cos\left(\frac{\pi}{3}\right) - \frac{m}{\sqrt{3}} \quad (2)$$

Where R_w – is the radius of the printing (working) zone, R – distance between the anchor and the geometric center of the print surface, h – distance to the AC chord, p – distance to the mass center of the equilateral triangle (nozzle support structure), L – length of the AC chord, m – nozzle support structure side length, and $\pi/3$ – half of the central angle. In this example, we assume that the ABC anchors, just like the corners of the nozzle support structure, are the vertices of equilateral triangles, and the printing bed origin coincides with the center of the circle circumscribed about the ABC anchors.

2.3. Operation and pre-printing tests

The hybrid printer is controlled by Pronterface software [49] installed on a computer. Slic3r open source software [50] converts 3D STL models into G-code toolpaths of the end effector.

After calibrating procedures, tests were carried out to determine the positioning accuracy, as well as the optimal temperature and speed modes. The positioning accuracy was determined by comparing the actual and defined coordinates along with two circles within the working area at the level of the printing surface. The optimal temperature and speed parameters were found by conducting a line test, where a single line, equivalent to the nozzle diameter, is printed over a wide range of temperatures (170-200oC) and printing speeds (5-30 mm/s).

Tensile tests were performed on pure 100% recycled PLA waste (Figure 5a), and it should be pointed out that mixtures of recycled and virgin plastic in various proportions can also be used (Figure 5b). Before printing, the shredded granules were dried in a vacuum chamber for 16 hours.

a) *b)*

Figure 5. Recycled PLA waste. a) 100% shredded PLA, b) combination of recycled (70%) and virgin PLA pellets (30%).

Preprints (www.preprints.org) | NOT PEER-REVIEWED | Posted: 3 August 2022 doi:10.20944/preprints202208.0075.v1

A standard Type-I ASTM: D638 tensile bar STL file was used [51] for producing the test specimens. The dimensions of the test specimen are 165x19x3.2 mm, which corresponds to four layers of 0.8 mm thickness with 100% infill. Considering the slicer parameters, the raster angle of the first layer was 0 degrees (print lines are perpendicular to the longitudinal axis), while for the remaining layers this angle was 90 degrees (print lines are parallel to the longitudinal axis).

In the Slic3r software the following settings were used to generate G-code:

- Filament diameter: 2.5 mm
- Extrusion multiplier: 1
- Temperature: 170°C
- Nozzle diameter: 1.5 mm
- Layer height: 0.7 mm
- Perimeters: 1
- Top solid layers: 1
- Bottom solid layers 1
- Quality settings:
    - Extra perimeters if needed
    - Avoid crossing perimeters
    - Detect thin walls
    - Detect bridging perimeters
- Seam position: aligned
- Infill density: 100%
- Infill overlap: 0%
- Infill pattern: rectilinear
- Print speed: 20 mm/s
- Travel speed: 40 mm/s
- First layer speed: 20 mm/s

Eight tensile bars were printed at the center (origin) of the printing bed. The printing location was then moved approximately 10 cm along the negative X axis of the printing bed, where an additional five bars were printed. Additionally, five bars were printed 10 cm along the positive X axis and five were printed 10 cm along the positive Y axis. All the tensile bars were printed parallel to the X axis.

3. Experimental results

The positioning accuracy was determined by comparing the actual and defined coordinates along with two circles within the working area at the level of the printing surface (Figure 6a). For the inner circle with the radius of 50 cm the positioning error is 0.58 ± 0.30 mm, and for the outer circle with the radius of 100 cm the error is 1.01 ± 0.90 mm. The results to find the optimal temperature and speed parameters are shown in Figure 6b, which illustrates the absolute difference between the actual and theoretical mass of the printed specimens.

Preprints (www.preprints.org) | NOT PEER-REVIEWED | Posted: 3 August 2022 doi:10.20944/preprints202208.0075.v1

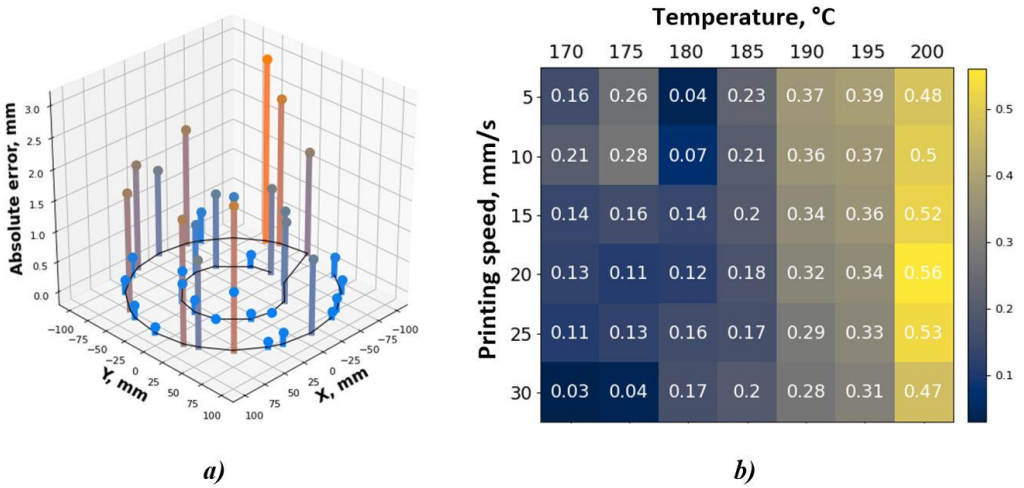

Figure 6. Positioning accuracy and mass accuracy of printed products. a) absolute positioning error at the printing bed level (in millimeters), b) absolute difference between the actual and theoretical weights of the test lines (in grams).

The results of preliminary tests show that positioning accuracy deteriorates as the nozzle moves away from the center of coordinates (origin point). Based on the ranges analyzed the optimal temperature and speed regimes lie within 170-175°C and 25-30 mm/s, respectively.

The results of the tensile tests performed on pure recycled PLA waste is shown in Figure 7. The Young's modulus for the samples printed at the origin, at the negative X, at the positive X, and the positive Y were 2.71 GPa, 2.27 GPa, 2.83 GPa and 2.66 GPa, respectively.

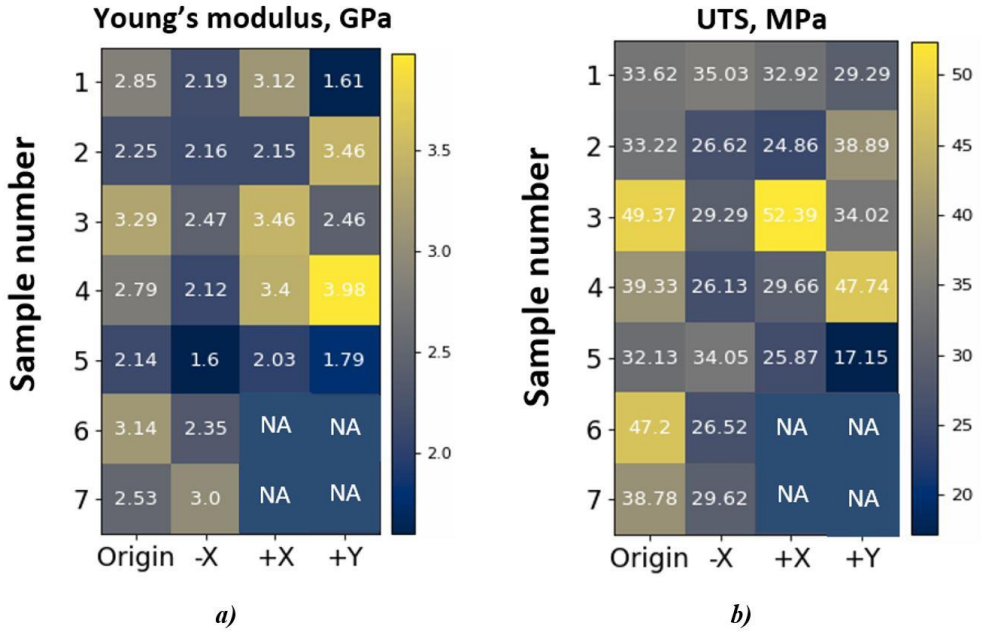

Figure 7. Young's modulus and Ultimate tensile strength of the printed specimens. a) Young's modulus (in GPa), b) Ultimate tensile strength (in MPa).

As previous studies have shown [52], the strength of plastic specimens varies greatly with changes in raster angle, moisture content, infill percentage, print direction, and other parameters. Brischetto and Torre [53] obtained Young's modulus in the range of 2.40-2.71 GPa for various families of ASTM D638 specimens, Pinto et al. [54] achieved 3.99 GPa for 80x21x0.43mm3 ASTM D882 PLA samples, Raj et al. [55] obtained 3.11 GPa mean Young's modulus for five ASTM D638 type V tensile samples, Algarni [56] measured modulus of elasticity in the range from 1.55 to 1.89 GPa for ASTM D638 tensile specimens with

Preprints (www.preprints.org) | NOT PEER-REVIEWED | Posted: 3 August 2022 doi:10.20944/preprints202208.0075.v1

different raster angles, and Grasso et al. [57] had maximum of ~2.9 GPa for 193x6x3 mm PLA samples. Zhao et al. [58] performed a comprehensive analysis for ISO 527-2-2012 155x20x4 mm tensile samples varying both printing angle and layer height. The obtained Young's moduli differ from 1.83 to 2.86 GPa for various sample families [58]. While some of the results here show a reduction in the Young's modulus of the highest values shown in the literature they are within most ranges of FFF and they are comparable to each other. This indicates that the location of a print on the print bed does not have a great effect on the modulus and hanging FPF is comparable to FFF/FDM.

The average value of the ultimate tensile strength (UTS) at the origin, negative X, positive X, and positive Y directions respectively were 39.09 MPa, 29.61 MPa, 33.14 MPa, and 33.42 MPA. These results indicate that specimens printed at the center of the hangprinter see a less significant drop in tensile strength than specimens printed at other places along the printer bed, which is caused by the positioning error (Figure 6).

These strength parameters can be compared with the results of previous studies. Laureto and Pearce [51] performed analysis for a large number of ASTM D638-14 types I and IV tensile geometries with various layer heights and print directions with maximum strength at ~60 MPa level. Alexandre et al. [24] conducted a comprehensive analysis of direct waste printing on an adapted desktop 3D printer. The results of tensile tests using ASTM D638 type IV samples showed that the shredded recycled material has characteristics comparable to the traditional FFF printing method, and the maximum strength can exceed 60 MPa24. Hanon et al. [52] obtained averaged strength range from 48.7 MPa to 58.4 MPa for ISO 527-2-2012 type 1B 150x10x4 mm specimens with different raster angles, Raj et al. [55] had 48.66 MPa mean strength for five ASTM D638 type V 63.5x9.53x3mm tensile samples, Brischetto and Torre53 measured the ultimate tensile strength within the range of 58.2-63.9 MPa for various families of ASTM D638 180x19x5 mm specimens, Zhao et al. [58] obtained 19.16-49.66 MPa UTS for ISO 527-2-2012 155x20x4 mm PLA samples with different layer thicknesses and printing orientation. The results were more striking for a reduction in tensile strength than those observed by Andreson (-10.9%)[59] and Sanchez et al.[60]. Thus, it can be argued that printing with a hangprinter shows consistent results, but the overall strength of the samples is inferior to traditional FFF manufacturing due to the large nozzle diameter, thick printing layers, and positioning inaccuracies.

In addition to tensile testing, consumer segment parts were manufactured to confirm printing quality. Figure 8 shows a DIY greenhouse corner bracket [61] that could be used for making cold frames and agrivoltaic test rigs [62].

Figure 8. Printing of consumer products example—greenhouse corner bracket with no post processing

Given the diameter of the nozzle and the thickness of the print lines, produced parts may require additional subtractive post-processing.

4. Discussion and future work

 doi:10.20944/preprints202208.0075.v1

This study successfully provided a proof-of-concept waste-based direct extrusion hangprinter, but there are substantial areas for future work. First, the mechanical properties of the prints were weaker than with other methods, which is due to non-uniform printing and high porosity that is the result of the weaker deposition accuracy of a heavy hangprinter head combined with non-uniform feedstock. Future work could develop a new version of the direct waste hangprinter using a smaller recyclebot-based motor and low-cost open source custom screws [63] based off of recyclebots rather than an FPF/FGF head. Second, the nature of the currently-used hangprinter design has a volume and shape limitation as the larger head can run into the cables. This problem can be overcome using a smaller form factor for the print head and having the hopper suspended above the printer feeding the print media with a flexible tube. A method is also needed to overcome the positioning error caused by calibration and to quantify the calibration accuracy as a function of the size of the hangprinter. There is obviously more research that needs to be put into using this type of hybrid FPF hangprinter with other polymer materials, as well as other materials and composites. Future work needs a way to auto calibrate the hangprinter with machine vision as well as use machine vision to auto correct print errors [64]. Finally, there is a need to fully optimize printing parameters and fix issues that cause increasing errors moving away from the center position.

5. Conclusions

This study has demonstrated the viability of an invention to use a waste plastic direct extrusion from a cable robot that has the potential to do DRAM for large quantities of waste and print large scale objects. Mechanical testing of the resultant prints, however, showed that combining challenges of non-uniform feedstocks and a heavy printhead for a hangprinter reduced the strength of the parts, which provides ample opportunities for researchers in the future to improve on the open source design to help process the volumes of waste plastic needed to address the negative environmental impacts of global plastic use.

Author Contributions: Conceptualization, JMP, BL and AP; methodology, JMP, BL and AP; validation, AP, BL, and RD; formal analysis, AP, BL, and RD; investigation, AP, BL, and RD; resources, JMP; data curation, AP, BL, and RD; writing—original draft preparation, AP, BL and RD; writing—review and editing, JMP; visualization, AP, BL, and RD; supervision, JMP; project administration, JMP; funding acquisition, JMP. All authors have read and agreed to the published version of the manuscript.

Funding: This work was supported by the Witte and Thompson Endowments.

Acknowledgments: The authors would like to thank Nagendra Tanikella for technical assistance and Torbjørn Ludvigsen for helpful discussions.

Conflicts of Interest: The authors declare no conflict of interest. The funders had no role in the design of the study; in the collection, analyses, or interpretation of data; in the writing of the manuscript; or in the decision to publish the results.

References

1. Kosior E, Crescenzi I. Solutions to the plastic waste problem on land and in the oceans. In Plastic waste and recycling 2020 Jan 1, pp. 415-446. Academic Press.
2. Faludi J, Cline-Thomas N, Agrawala S. 3D printing and its environmental implications. In: The Next Production Revolution: Implications for Governments and Business, OECD Publishing, 2017, Paris, France, ch. 5, pp. 171-213. https://doi.org/10.1787/9789264271036-en.
3. Bowyer A. 3D printing and humanity's first imperfect replicator. 3D printing and additive manufacturing 2014, 1(1), 4-5.
4. Barrett A. Is PLA Recyclable? 2020. https://bioplasticsnews.com/2020/04/05/is-pla-recyclable. (accessed 08 March 2022).
5. Globe Newswire. The Market for Additive Manufacturing in the Oil and Gas Sector 2018-2029. 2019. https://www.globenewswire.com/news-release/2019/06/04/1864243/0/en/NewSmarTech-Analysis-Report-on-Additive-Manufacturing-in-the-Oil-and-Gas-IndustryFinds-1B-Opportunity-for-AM-Hardware-Manufacturers.html. (accessed 08 March 2022).

6. Zhong S, Pearce JM. Tightening the loop on the circular economy: Coupled distributed recycling and manufacturing with recyclebot and RepRap 3-D printing. Resour. Conserv. Recycl. 2018. 128, 48–58. https://doi.org/10.1016/j.resconrec.2017.09.023.
7. Santander P, Sanchez FAC, Boudaoud H, & Camargo M. Closed loop supply chain network for local and distributed plastic recycling for 3D printing: a MILP-based optimization approach. Resour. Conserv. Recycl. 2020, 154, 104531.
8. Sanchez FAC, Boudaoud H, Camargo M, Pearce JM. Plastic recycling in additive manufacturing: A systematic literature review and opportunities for the circular economy. J. Clean. Prod. 2020, 264, 121602. https://doi.org/10.1016/j.jclepro.2020.121602.
9. Pavlo S, Fabio C, Hakim B, Mauricio C. 3D-Printing Based Distributed Plastic Recycling: A Conceptual Model for Closed-Loop Supply Chain Design. In Proceedings of the 2018 IEEE International Conference on Engineering, Technology and Innovation (ICE/ITMC), 2018, Stuttgart, Germany, pp. 1–8.
10. Dertinger SC, Gallup N, Tanikella NG et al. Technical pathways for distributed recycling of polymer composites for distributed manufacturing: Windshield wiper blades. Resour. Conserv. Recycl. 2020, 157, 104810.
11. Kreiger MA, Mulder ML, Glover AG, & Pearce JM. Life cycle analysis of distributed recycling of post-consumer high density polyethylene for 3-D printing filament. J. Clean. Prod. 2014, 70, 90-96.
12. Kreiger M & Pearce JM. Environmental life cycle analysis of distributed three-dimensional printing and conventional manufacturing of polymer products. ACS Sustainable Chemistry & Engineering 2013, 1(12), 1511-1519.
13. Gwamuri J, Wittbrodt BT, Anzalone NC & Pearce JM. Reversing the trend of large scale and centralization in manufacturing: The case of distributed manufacturing of customizable 3-D-printable self-adjustable glasses. Challenges in Sustainability 2014, 2(1), 30-40. DOI: 10.12924/cis2014.02010030.
14. Petersen EE & Pearce JM. Emergence of home manufacturing in the developed world: Return on investment for open-source 3-D printers. Technologies 2017, 5(1), 7. https://doi.org/10.3390/technologies5010007
15. Mohammed M, Wilson D, Gomez-Kervin E et al. Sustainability and feasibility assessment of distributed E-waste recycling using additive manufacturing in a Bi-continental context. Additive Manufacturing 2022, 50, 102548. https://doi.org/10.1016/j.addma.2021.102548.
16. Laplume AO, Petersen B, Pearce JM. Global value chains from a 3D printing perspective. J. Int. Bus. Stud. 2016, 47, 595–609. https://doi.org/10.1057/jibs.2015.47.
17. Zhong S, Rakhe P & Pearce JM. Energy payback time of a solar photovoltaic powered waste plastic recyclebot system. Recycling 2017, 2(2), 10.
18. Woern AL, McCaslin JR, Pringle AM, Pearce JM. RepRapable Recyclebot: Open source 3-D printable extruder for converting plastic to 3-D printing filament. HardwareX 2018, 4, e00026, https://doi.org/10.1016/j.ohx.2018.e00026.
19. Woern AL, Byard DJ, Oakley RB et al. Fused particle fabrication 3-D printing: Recycled materials' optimization and mechanical properties. Materials 2018, 11(8), 1413. https://doi.org/10.3390/ma11081413.
20. Little HA, Tanikella NG, Reich MJ et al. Towards distributed recycling with additive manufacturing of PET flake feedstocks. Materials 2020, 13(19), 4273.
21. Reich MJ, Woern AL, Tanikella NG & Pearce JM. Mechanical properties and applications of recycled polycarbonate particle material extrusion-based additive manufacturing. Materials 2019, 12(10), 1642.
22. Volpato N, Kretschek D, Foggiatto JA & Gomez da Silva Cruz CM. Experimental analysis of an extrusion system for additive manufacturing based on polymer pellets. The International Journal of Advanced Manufacturing Technology 2015, 81(9), 1519-1531.
23. Whyman S, Arif KM & Potgieter J. Design and development of an extrusion system for 3D printing biopolymer pellets. The International Journal of Advanced Manufacturing Technology 2018, 96(9), 3417-3428.
24. Alexandre A, Sanchez FAC, Boudaoud H et al. Mechanical properties of direct waste printing of polylactic acid with universal pellets extruder: comparison to fused filament fabrication on open-source desktop three-dimensional printers. 3D Printing and Additive Manufacturing 2020, 7(5), 237-247.
25. Byard DJ, Woern AL, Oakley RB et al. Green fab lab applications of large-area waste polymer-based additive manufacturing. Additive Manufacturing 2019, 27, 515-525.
26. Gigabot XLT (re3d), https://re3d.org/portfolio/gigabot-xlt. (accessed 08 March 2022).
27. Exabot (re3d), https://re3d.org/portfolio/exabot. (accessed 08 March 2022).
28. Terabot (re3d), https://re3d.org/portfolio/terabot. (accessed 08 March 2022).
29. THE BOX Large (BLB Industries), https://www.aniwaa.com/product/3d-printers/blb-industries-the-box-large. (accessed 08 March 2022).
30. T3500 (Tractus3D), https://www.aniwaa.com/product/3d-printers/tractus3d-t3500-rtp. (accessed 08 March 2022).
31. 400 Series WORKBENCH XTREME (3D Platform), https://www.aniwaa.com/product/3d-printers/3d-platform-400-series-workbench-xtreme. (accessed 08 March 2022).
32. BIG-Meter (Modix), https://www.aniwaa.com/product/3d-printers/modix-big-meter. (accessed 08 March 2022).
33. BigRep ONE v4 (BigRep), https://www.aniwaa.com/product/3d-printers/bigrep-one. (accessed 08 March 2022).
34. F1000 (CreatBot), https://www.aniwaa.com/product/3d-printers/creatbot-f1000. (accessed 08 March 2022).
35. Ludvigsen T, Kracht P. Clerck, a RepRap 3D printer hanging from the ceiling. Appropedia 2006. https://www.appropedia.org/Clerck,_a_RepRap_3D_printer_hanging_from_the_ceiling (accessed 08 March 2022).

36. Bruckmann T, Mickelsons L, Brandt T et al. Wire robots part I - kinematics, analysis and design. In Parallel Manipulators - New Developments, ARS Robotic Books, Vienna, Austria, 2008. I-Tech Education and Publishing.
37. Saber O. A Spatial Translational Cable Robot. ASME. J. Mechanisms Robotics 2015, 7(3): 031006. https://doi.org/10.1115/1.4028287.
38. Zhong Y and Qian S. A Cable-Driven Parallel Robot for 3D Printing, 2018 IEEE International Conference on Mechatronics, Robotics and Automation (ICMRA), 2018, pp. 199-203, https://doi.org/10.1109/ICMRA.2018.8490542.
39. Zi B, Wang N, Qian S & Bao K. Design, stiffness analysis and experimental study of a cable-driven parallel 3D printer. Mechanism and Machine Theory 2019, 132, 207-222.
40. Vu DS, Barnett E & Gosselin C. Experimental validation of a three-degree-of-freedom cable-suspended parallel robot for spatial translation with constant orientation. Journal of Mechanisms and Robotics 2019, 11(2).
41. Chesser PC, Wang PL, Vaughan JE et al. Kinematics of a Cable-Driven Robotic Platform for Large-Scale Additive Manufacturing. Journal of Mechanisms and Robotics 2022, 14(2).
42. Daren S. Arcus-3D-C1—Cable 3D printer. 2017. https://hackaday.io/project/26938-arcus-3d-c1-cable-3d-printer (accessed 14 December 2021).
43. Sensorica: SpiderRig, 2012. https://www.sensorica.co/ventures/robotics-and-fabrication/spiderrig (accessed 08 March 2022).
44. Trikarus Project, 2021. https://stadtfabrikanten.org/pages/viewpage.action?pageId=72122510 (accessed 08 March 2022).
45. Ludvigsen, T. Hangprinter v3 Manual. https://hangprinter.org/doc/v3/ (accessed 08 March 2022).
46. Ludvigsen, T. Hangprinter v3 firmware. 2018. https://github.com/tobbelobb/hangprinter/tree/Openscad_version_3/firmware (accessed 08 March 2022).
47. Pearce JM, Lavu B, Dick, Petsiuk A and Rattan R. Waste Plastic Direct Extrusion Hangprinter. OSF. 2021. osf.io/jgb8z. (accessed 08 March 2022).
48. RAMPS 1.4. https://reprap.org/wiki/RAMPS_1.4, 2021 (accessed 08 March 2022). .
49. Printrun: 3D printing host suite. https://www.pronterface.com/ (accessed 08 March 2022).
50. Slic3r: Open source 3D printing toolbox. https://slic3r.org/ (accessed 08 March 2022).
51. Laureto JJ & Pearce JM. Anisotropic mechanical property variance between ASTM D638-14 type i and type iv fused filament fabricated specimens. Polymer Testing 2018, 68, 294-301.
52. Hanon MM, Marczis R and Zsidai L. Influence of the 3D Printing Process Settings on Tensile Strength of PLA and HT-PLA. Periodica Polytechnica Mechanical Engineering 2021, 65, 1 (2021), 38–46. https://doi.org/10.3311/PPme.13683.
53. Brischetto S, Torre R. Tensile and Compressive Behavior in the Experimental Tests for PLA Specimens Produced via Fused Deposition Modelling Technique. Journal of Composites Science. 2020, 4(3):140. https://doi.org/10.3390/jcs4030140.
54. Pinto VC, Ramos T, Alves S et al. Comparative Failure Analysis of PLA, PLA/GNP and PLA/CNT-COOH Biodegradable Nanocomposites thin Films. Procedia Engineering 2015, v. 114, pp. 635-642. https://doi.org/10.1016/j.proeng.2015.08.004.
55. Raj SA, Muthukumaran E, and Jayakrishna K. A Case Study of 3D Printed PLA and Its Mechanical Properties. Materials Today: Proceedings 2018, 5(5-2), pp. 11219-11226. https://doi.org/10.1016/j.matpr.2018.01.146.
56. Algarni M. The Influence of Raster Angle and Moisture Content on the Mechanical Properties of PLA Parts Produced by Fused Deposition Modeling. Polymers 2021, 13, 237. https://doi.org/10.3390/polym13020237.
57. Grasso M, Azzouz L, Ruiz-Hincapie P et al. Effect of temperature on the mechanical properties of 3D-printed PLA tensile specimens. Rapid Prototyping Journal 2018, 24(8), pp. 1337-1346. https://doi.org/10.1108/RPJ-04-2017-0055.
58. Zhao Y, Chen Y, Zhou Y. Novel mechanical models of tensile strength and elastic property of FDM AM PLA materials: Experimental and theoretical analyses. Materials & Design 2019, v. 181, 108089. https://doi.org/10.1016/j.matdes.2019.108089.
59. Anderson I. Mechanical properties of specimens 3D printed with virgin and recycled polylactic acid. 3D Printing and Additive Manufacturing 2017, 4(2), 110-115.
60. Sanchez FAC, Lanza S, Boudaoud H, Hoppe S, & Camargo M. (2015). Polymer Recycling and Additive Manufacturing in an Open Source context: Optimization of processes and methods. In Annual international solid freeform fabrication symposium, ISSF 2015 (pp. 1591-1600).
61. DIY modular greenhouse, https://www.prusaprinters.org/prints/62627-diy-greenhouse-by-kms (accessed 08 March 2022).
62. Pearce JM. Parametric Open Source Cold-Frame Agrivoltaic Systems. Inventions 2021, 6(4), p.71. https://doi.org/10.3390/inventions6040071
63. Franz J & Pearce JM. Open-source grinding machine for compression screw manufacturing. Inventions 2020, 5(3), 26.
64. Petsiuk A & Pearce JM. Towards Smart Monitored AM: Open Source in-Situ Layer-wise 3D Printing Image Anomaly Detection Using Histograms of Oriented Gradients and a Physics-Based Rendering Engine. Additive Manufacturing 2022, 52, 102690. https://doi.org/10.1016/j.addma.2022.102690.